PAPER

Model-based design of a multistable origami-enabled crawling robot

IOP Publishing Smart Materials and Structures
Smart Mater. Struct. **29** (2020) 015013 (9pp) https://doi.org/10.1088/1361-665X/ab52c5

Model-based design of a multistable origami-enabled crawling robot

Kim Gustafson, Oyuna Angatkina and Aimy Wissa

University of Illinois at Urbana-Champaign, Urbana, IL, United States of America

E-mail: awissa@illinois.edu

Received 20 May 2019, revised 20 September 2019
Accepted for publication 30 October 2019
Published 29 November 2019

Abstract

Origami and kirigami are becoming increasingly more prevalent in robotic systems due to their elegant manufacturability and pseudo-compliant behavior. However, origami-enabled robotic systems are currently designed in an inefficient ad hoc manner due to the complexity of synergistically incorporating compliant origami structures into a system level model. This paper develops a system level dynamic model for the locomotion of an origami-enabled crawling robot. An energy analysis of the primary mechanical components of the robot yields a one-dimensional (1D) equation of motion (EOM) for the robot. The EOM is extended to two dimensions (2D) using a geometric analysis of the origami structures and the constraints imposed by the robotic system. The 2D model is able to represent the robot's forward and directional locomotion. The results of the dynamic model are compared to a kinematics-based model and experimental results. The 2D dynamic model performs similar to the kinematic model of the robot for small forward expansions, but the dynamic model demonstrates superior tracking of the robot locomotion for larger expansions as the system losses increase. The maximum error reported between the dynamic model and experimental results is 10% compared to the 40% error reported for the kinematic model. The paper concludes with a demonstration of how the dynamic model can be used to select the robot design parameters. This paper presents a much-needed framework for the design of origami-enabled robots that can also lead to advances in the control of compliant and pseudo-compliant robots.

Supplementary material for this article is available online

Keywords: origami robots, multistable origami, model-based design, kresling origami, crawling robots

(Some figures may appear in colour only in the online journal)

Nomenclature

β	Rotation of single cell model at origami relief cuts	ϕ_L	Rotational input to left origami tower of robot
F_{cell}	Force applied by single origami cell	ϕ_R	Rotational input to right origami tower of robot
F_{tower}	Force applied by origami tower	r	Length of link formed by two adjacent origami cells
$k_{bellows}$	Stiffness of bellows structure	μ	Friction coefficient of robot feet
l_{plate}	Distance between origami towers at end plates	X	Global lateral robot expansion
m	Mass of crawling robot front plate	X_f	Position of robot front plate centroid in X direction
ϕ	Rotational input to origami	y	Forward robot expansion for single cell model
		y_0	Initial bellows offset

$\boldsymbol{Y}$	Global forward robot expansion
$\boldsymbol{Y_f}$	Position of robot front plate centroid in $\boldsymbol{Y}$ direction

1. Introduction

Recent interest in employing origami and kirigami as components in robotic systems stems from their elegant manufacturability and pseudo-compliant behavior [1]. While much effort has been extended towards developing geometric and mechanical models for individual origami structures, very little work has been done to quantitatively establish models for origami-enabled robots that synergistically integrate the origami structures into a system level model [2]. This paper establishes a model for the locomotion of a crawling robot enabled by multistable origami structures through an investigation of the system level dynamics of the robot. The crawling robot considered in this paper [3] is a case study for a modeling framework that can be generalized to other origami-enabled robotic systems. The paper also demonstrates how the model can be used to efficiently tune the robot design parameters and replace the ad hoc methods currently used to design complex origami-enabled robotic systems.

Many techniques have been developed for modeling the kinematics of origami structures, including the Miura-Ori pattern [4–7], the Kresling pattern [3, 8, 9], and the water-bomb unit [10]. In addition to the kinematics of origami structures, there has been significant focus directed towards the actuation of origami structures using pneumatic actuation [10, 11] and smart actuators such as shape memory alloys [2, 12, 13]. These actuation methods have been studied for both the locomotion and self-folding of origami-enabled robots [14–16]. However, after an extensive review of origami-enabled robots, Rus and Tolley have determined there is a need for realistic physical models that can better inform the control algorithms of origami-enabled robots for task execution [1]. Zhakypov and Paik, who have developed a systematic design methodology for building origami-inspired robots, similarly concluded there is a lack of standard models for origami-enabled robots that can be synergistically integrated into a design tool for origami robotic systems [2].

This paper addresses the need for a system level model of origami-enabled robots that can be used to aid in the design of the robotic systems. The paper begins with an overview of the origami-enabled robotic platform, Peri and a breakdown of the robot's primary locomotion components. Hamilton's equation is used to derive an equation of motion (EOM) for the robot, and the robot locomotion predicted by this dynamic model is compared to the locomotion predicted by a kinematic model of the robot. The dynamic model results are validated against experimental measurements for both forward (one-dimensional (1D)) and directional (two-dimensional (2D)) locomotion. The paper concludes with a discussion of how the dynamic model can be used to efficiently tune the robot design parameters to achieve desired performance requirements, creating a much-needed framework for the design of origami-enabled robots.

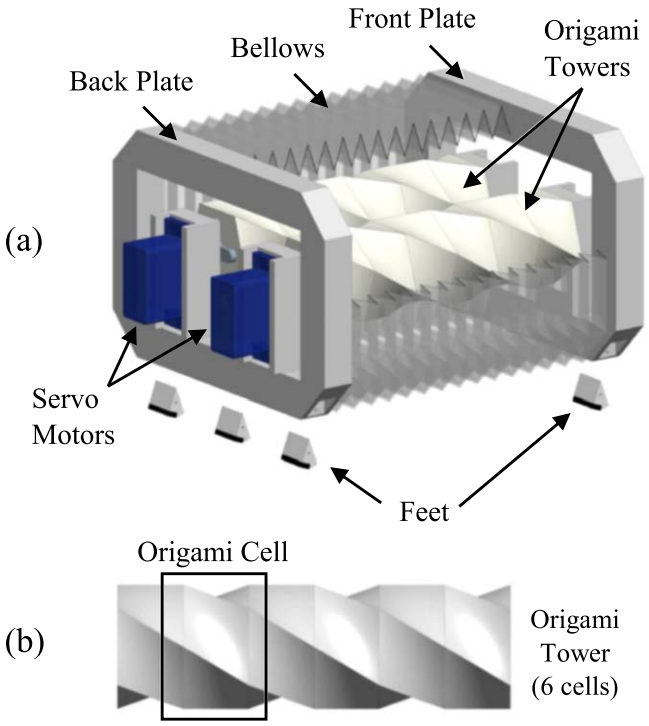

Figure 1. (a) Rendering of the origami-enabled crawling robot, Peri. The primary mechanical locomotion components of Peri include two rigid plates connected by two origami towers actuated independently using servo motors. Anisotropic feet allow the robot to move forward without slipping as the origami towers expand and contract. (b) Origami tower of Peri constructed from 6 origami Kresling cells.

2. Characterization of robotic platform components

The dynamic model developed in this paper is tailored for the origami-enabled crawling robot, Peri [3]. Peri is a bio-inspired pseudo-compliant robot that mimics the anterograde locomotion of the caterpillar. The primary mechanical locomotion components of Peri are identified in figure 1(a). Two rigid end plates are linked by origami towers actuated independently using servo motors. By nature of the Kresling origami pattern [3], the towers expand and contract as a rotation is applied to one end of the towers, with the other end fixed. Figure 1(b) shows an origami tower of Peri constructed from six origami Kresling cells. Two origami towers in parallel allow for directional locomotion (i.e. left and right turning). A transparent PTE bellows structure supplies torsional rigidity between the front and back plates and provides protection for the origami towers. Anisotropic feet allow the robot to expand and contract with no backwards slipping [17].

While the design of Peri has been detailed in [3, 17], the primary components of the robot have not been characterized individually. Thus, three experiments have been conducted to characterize the origami towers, bellows structure, and anisotropic feet of the crawling robot.

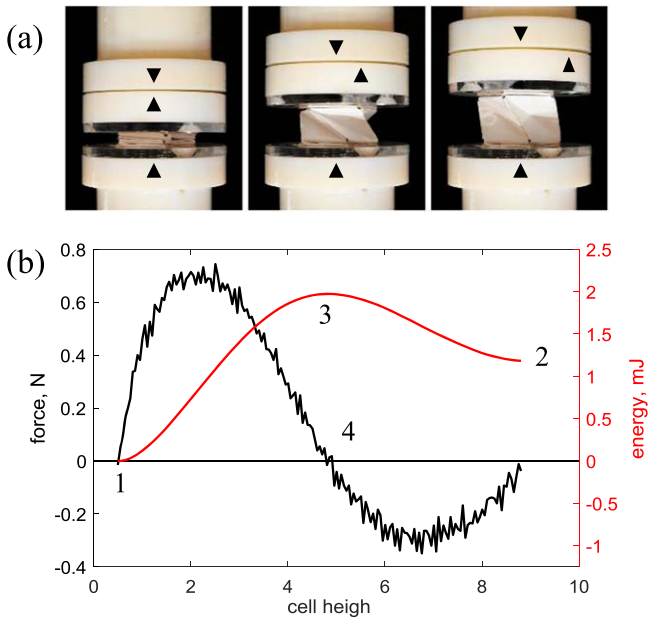

Figure 2. (a) Characterization of a Kresling cell using a universal testing machine with a fixture that allows for rotation of one end of the cell. A constant displacement was applied to expand the cell, and the corresponding force was recorded. (b) Measured force–displacement profile that demonstrates the bistability of the cell. The energy, a numerical integral of the force data, shows the two stable equilibrium positions of the cell (1) and (2), the unstable equilibrium (3), and the snap through height where the force is zero (4).

2.1. Origami towers

The origami towers that enable the crawling locomotion of Peri are constructed from six repeating cells of the Kresling origami pattern [3]. Each Kresling cell exhibits the force-displacement behavior presented in figure 2(b), obtained using a universal testing machine. A fixture that allows one end of the cell to rotate during expansion was used to mount the cell to the universal testing machine as shown in figure 2(a).

The cell was pulled with a constant velocity of 1 mm s^{-1}, and the corresponding reaction force was measured (see supplementary video M1, available online at stacks.iop.org/SMS/29/015013/mmedia). The energy profile of the cell presented in figure 2(b) was obtained by numerically integrating the force-displacement data measured by the universal testing machine. The energy profile shows the bistability of the Kresling cell, with two stable equilibrium positions at (1) and (2). The unstable equilibrium where the energy is a maximum (3) represents the cell critical height at which snap through occurs, indicated by a measured force value of zero (4).

2.2. Bellows structure

The primary functions of the bellows structure are to provide torsional rigidity to the crawling robot and protect the origami towers. The free length of the bellows is greater than the maximum distance between the front and back plates of the robot during expansion. This indicates that the bellows always operates under compression and assists the forward

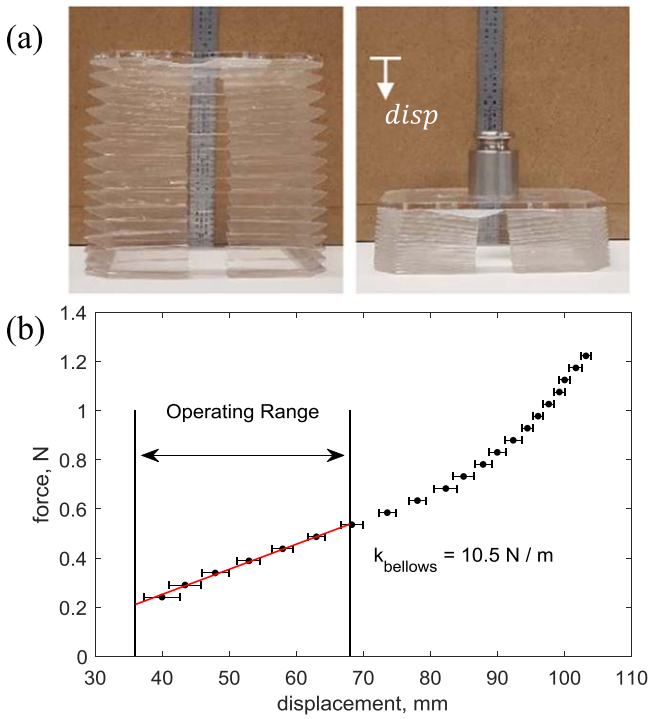

Figure 3. (a) Bellows structure characterization setup. Discrete weights were applied to compress the bellows (free length of 130 mm), and the resulting displacements were measured using the scale shown. (b) The bellows stiffness of 10.5 N m^{-1} was calculated from a linear fit of the experimentally determined operating range. Loads and displacements were defined positive downwards, and the force-displacement data represents the mean of 3 trials.

locomotion of the robot. The force-displacement behavior of the bellows structure was determined experimentally by applying weights to the bellows and measuring the resulting compression, as shown in figure 3(a). While the bellows reponse was nonlinear as shown in figure 3(b), the displacement represented by the operating range of the crawling robot was reasonably approximated as linear. The average bellows stiffness from the linear operating range of the structure was measured across three trials to be 10.5 N m^{-1}.

2.3. Anisotropic feet

The expanding and contracting locomotion of Peri is enabled by anisotropic feet allowed to pivot about a central axle as shown in figure 4. As the robot expands, the hind feet rotate to a high friction surface to prevent the robot from slipping backwards, while the front feet rotate to a low friction surface to allow expansion. Similarly, as the robot contracts, the front feet rotate to the high friction surface and the hind feet rotate to the low friction surface, allowing the back plate to contract to the front plate with no slipping. The feet are 3D printed using a Stratasys Objet printer from print materials VeroWhite (low friction) and TangoBlack (high friction).

Perfect stiction is assumed for the high friction material to prevent backwards slipping. The coefficient of friction for the low friction material was measured by placing a known weight on a sample of the low friction material (VeroWhite) and applying a lateral force in the forward locomotion

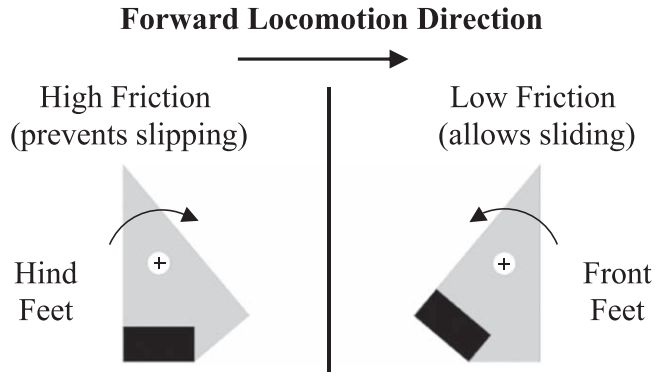

Figure 4. Anisotropic feet allow sliding for forward robot locomotion but prevent backwards slipping. The low friction material has experimentally measured static coefficient of friction $\mu = 0.51$. Perfect stiction (no slipping) is assumed for the high friction material.

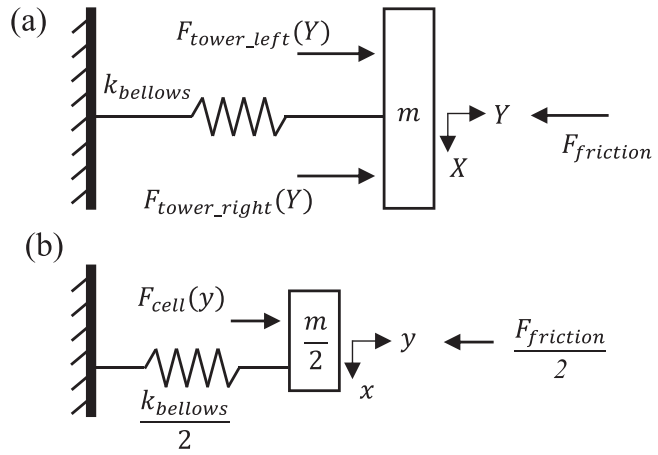

Figure 5. (a) Idealized model of the robot Peri during expansion, where the back plate is fixed, and all loads are applied to the robot front plate. The bellows is modeled as an undamped linear spring, friction as a negative external force, and each origami tower as a positive position-dependent external force. (b) Idealized schematic of the single-cell model acting on half of the front plate mass, where y is the front plate position for the expansion of a single origami cell.

direction. The applied force required to overcome static friction and the normal force were used to determine the coefficient of friction using a Coulomb model. The measured static coefficient of friction for VeroWhite is 0.51.

3. Dynamic model formulation

The dynamic model of Peri is developed from an energy analysis of the mechanical components of the robot characterized in section 2. Figure 5(a) shows an idealized model of the crawling robot during expansion, where the back plate is fixed, and the system forces are applied to the robot front plate of mass m.

The bellows structure is modeled as an undamped linear compression spring with stiffness $k_{bellows}$, and all structural damping is considered negligible. $F_{friction}$ is the external force applied to the front plate by the low friction material of the robot feet. The static coefficient of friction measured in section 2.3, $\mu = 0.51$, is used for both the static coefficient of friction and as a conservative estimate of the kinetic coefficient of friction for the model formulation. Each origami tower is represented by the position dependent force, F_{tower}, applied to the front plate, and X and Y are the transverse and longitudinal positions of the front plate, respectively. The model assumes that the forward displacement of the front plate, referred to as expansion, is equivalent to the forward locomotion of the robot and that contraction is a perfect reversal of expansion.

3.1. Single cell model

Due to the metameric nature of the origami towers, a model is initially developed for the dynamic response of a single origami cell. Figure 5(b) is the idealized model for a single origami cell of the robot. Each cell belongs to one origami tower, and each tower is idealized to apply a force to one half of the front plate. Thus, for the single cell model, each Kresling cell is assumed to apply a force directly to one half of the front plate that is transmitted through all other Kresling cells. Similarly, only one half of the friction force and one half of the bellows stiffness are considered. In figure 5(b), y is the position in the direction of forward expansion for a single origami cell of the robot, and x is the transverse position for a single origami cell.

3.1.1. Single cell model design. The EOM for the origami-enabled crawling robot is obtained from an energy analysis of the primary locomotion components using Hamilton's equation

$$\int_{t_1}^{t_2} [\delta(T - V) + \delta W_{nc}]dt = 0, \tag{1}$$

where T and V are the kinetic and potential energy of the system, respectively, and W_{nc} is the work from all nonconservative forces acting on the system. The origami is modeled as a position-dependent force applied to the robot front plate and expressed by

$$W_{cell} = F_{cell}(y) * y, \tag{2}$$

where $F_{cell}(y)$ is the force-displacement profile obtained for the Kresling cell presented in figure 2(b). The friction force applied to the robot front plate is modeled using a Coulomb friction model

$$W_{friction} = \mu \frac{m}{2} g y, \tag{3}$$

where g is the acceleration due to gravity, and μ is the coefficient of friction for the low friction material of the anisotropic feet. The bellows is modeled as a linear spring with potential energy

$$V_{bellows} = \frac{1}{4} k_{bellows}(y + y_0)^2, \tag{4}$$

where y_0 is the initial bellows offset, which was determined experimentally for Peri. Substituting the energy expressions for the primary robot locomotion components given by equations (2)–(4) into Hamilton's equation yields the

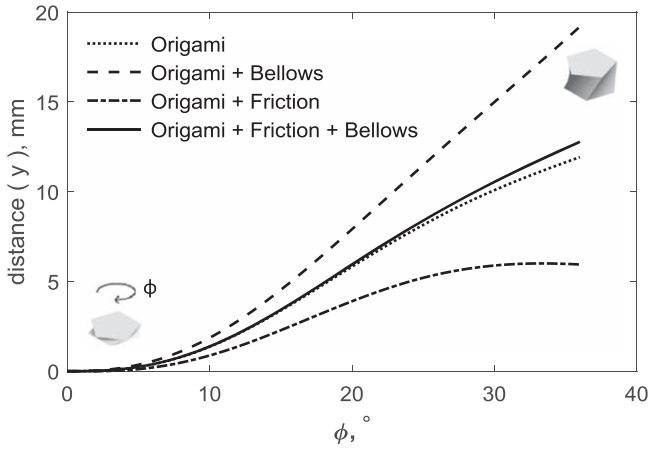

Figure 6. Forward expansion of the robot front plate from a single Kresling cell as a function of the input rotation ϕ supplied to the cell. The legend indicates each component included in the dynamic model for the corresponding solution (i.e. for the Origami + Bellows case, the ODE given by equation (5) is solved for $\mu = 0$).

following EOM expressed in state space form:

$$\begin{Bmatrix} \dot{y}_1 \\ \dot{y}_2 \end{Bmatrix} = \begin{bmatrix} 0 & 1 \\ \frac{k_{bellows}}{m} & 0 \end{bmatrix} \begin{Bmatrix} y_1 \\ y_2 \end{Bmatrix} + \begin{bmatrix} 0 \\ \frac{1}{m} \end{bmatrix} (F_{cell}(y) - \mu mg + k_{bellows} y_0). \tag{5}$$

The EOM for the single cell model is solved using the MATLAB solver ODE45. The solution is converted from a function of time to a function of the servo input rotation, ϕ, using the angular velocity of the servo motors.

3.1.2. Single cell model results. Figure 6 presents the 1D expansion of the robot front plate as a function of the rotation, ϕ, input to a single origami cell. The EOM given by equation (5) is solved for various combinations of the robot components to show the effect of each component on the front plate expansion. The solution is first presented for only the force of the origami cell applied to the robot front plate (i.e. $\mu = k_{bellows} = 0$). The solution is then presented for only the origami force and the bellows (i.e. $\mu = 0$), and then for only the origami and friction forces (i.e. $k_{bellows} = 0$). The solution for all components is used to construct the full robot model in section 3.2.

As mentioned previously and presented in figure 3, the bellows operates under compression for the full operating range of the robot, meaning that the bellows assists the forward locomotion of the robot. For the specific design configuration of Peri, the bellows and friction terms nearly cancel, making the solution for all components very similar to that of just the origami force acting on the front plate. However, this response would not necessarily be observed for other parameter values or system design configurations.

3.2. Full robot model

3.2.1. Full robot model assembly. The Kresling origami cell expands strictly in 1D for a given input rotation, ϕ. To allow for directional (2D) robot locomotion, relief cuts [3] are added between every set of adjacent Kresling cells for the construction of the origami towers of Peri as shown in figure 7(a). Each relief cut is modeled as a pin joint, and each set of adjacent Kresling cells is modeled as a variable length rigid link, $\vec{r}_j$, whose length is the summation of the single cell model solution for the two cells of the link (i.e. $r_1 = y_{cell1} + y_{cell2}$). Each link is defined at an angle β_j from the positive Y direction of the robot coordinate system, as shown in figure 7(b).

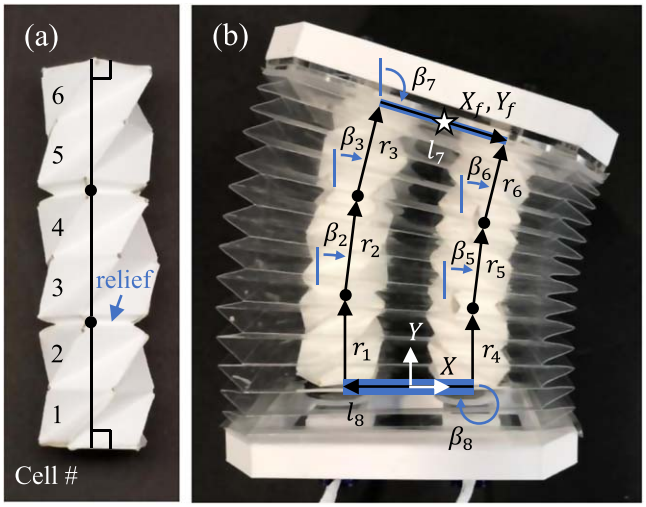

Figure 7. (a) Origami tower constructed from 6 Kresling cells, with a relief joint between every set of adjacent cells. Each relief is modeled as a pin joint, and each set of adjacent cells is modeled as a rigid link of variable length $\boldsymbol{r_j}$. The ends of the tower are constrained to be perpendicular to the front and back plates of the robot. (b) Each link $\vec{\mathbf{r}}_\mathbf{j}$ is at an angle $\beta_\mathbf{j}$ with respect to the robot coordinate system $\boldsymbol{X}$, $\boldsymbol{Y}$. The length of each link, $\boldsymbol{r_j}$, corresponds to the single cell model solution of the two cells that make up the link. $\boldsymbol{X_f}$, $\boldsymbol{Y_f}$ represents the global position of the robot front plate.

Due to the boundary conditions of the origami towers, the origami cells are assumed to snap from the center of the towers, where the cells are the least constrained, outwards, with one cell expanding completely before the next cell begins to expand. This snapping order was confirmed through several experimental observations (supplementary video M2). The link lengths, r_j, are known from the input servo rotations, the cell snapping order, and the single cell model results for each cell. The link orientations, β_j, are determined using the following vector loop equations in X and Y, respectively:

$$r_1 \sin\beta_1 + r_2 \sin\beta_2 + r_3 \sin\beta_3 - r_4 \sin\beta_4 - r_5 \sin\beta_5 - r_6 \sin\beta_6 + l_7 \sin\beta_7 + l_8 \sin\beta_8 = 0 \tag{6}$$

$$r_1 \cos\beta_1 + r_2 \cos\beta_2 + r_3 \cos\beta_3 - r_4 \cos\beta_4 - r_5 \cos\beta_5 - r_6 \cos\beta_6 + l_7 \cos\beta_7 + l_8 \cos\beta_8 = 0, \tag{7}$$

subject to the constraints

$$\beta_1 = \beta_4 = \beta_8 - \pi/2 = 0, \tag{8}$$

$$\beta_3 = \beta_6 = \beta_7 + \pi/2, \tag{9}$$

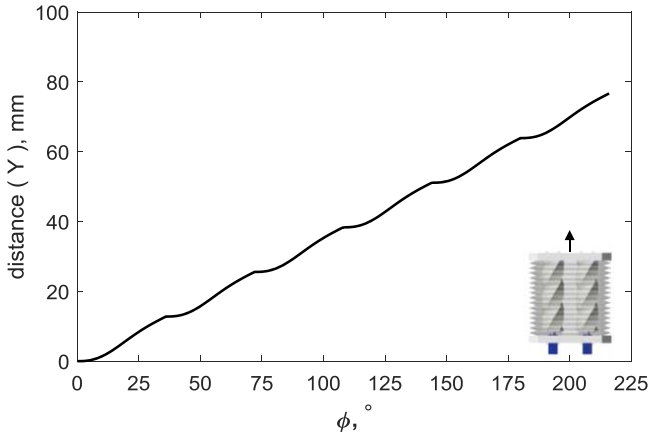

Figure 8. Forward (1D) expansion in the $\boldsymbol{Y}$ direction for the full robot model as a function of the servo motor rotations, ϕ, where $\phi_L = \phi_R$. The forward expansion profile assumes an identical snapping order for the cells of the right and left origami towers.

and

$$\beta_2 = \beta_5, \tag{10}$$

where β_7 and β_8 are the orientations of the front and back plates, respectively, and $l_7 = l_8 = 44$ mm is the distance between the left and right origami towers at the end plates. Equations (8) and (9) constrain the ends of the origami towers to be perpendicular to the end plates and define the robot coordinate system, X, Y, at the center of the back plate as shown in figure 7(b). Equation (10) is a geometric constraint imposed by the vector loop design. The solution of the vector loop analysis yields all β_j and fully defines the front plate position (X_f, Y_f). The full robot model uses the single cell model combined with the vector loop analysis to output the 2D position of the robot front plate, X_f, Y_f, from the servo rotations input to the left (ϕ_L) and right (ϕ_R) origami towers.

3.2.2. Full robot model results. Figure 8 presents the full robot model results for forward (1D) expansion in the Y direction, where $\phi_L = \phi_R = \phi$. Due to the assumption that the origami cells snap one after another, the expansion profile of figure 8 is a sequential repetition of the single cell model profile for all components presented in figure 6. The forward expansion results presented in figure 8 assume an identical cell snapping order for the left and right origami towers of the robot.

The results of the full robot model for directional (2D) expansion are presented in figure 9. Each path represents the displacement of the robot front plate for one expansion of the robot moving forward or turning left or right. The origami cell snapping order is assumed to be from the center of the towers outwards, and the turning profiles are given by $\phi_R = 2\phi_L$ and $\phi_L = 2\phi_R$ for turning left and right, respectively.

4. Model validation and verification

The dynamic model results presented in section 3 are compared to results from a kinematic model of the robot and validated against experimental data collected from the robotic platform, Peri.

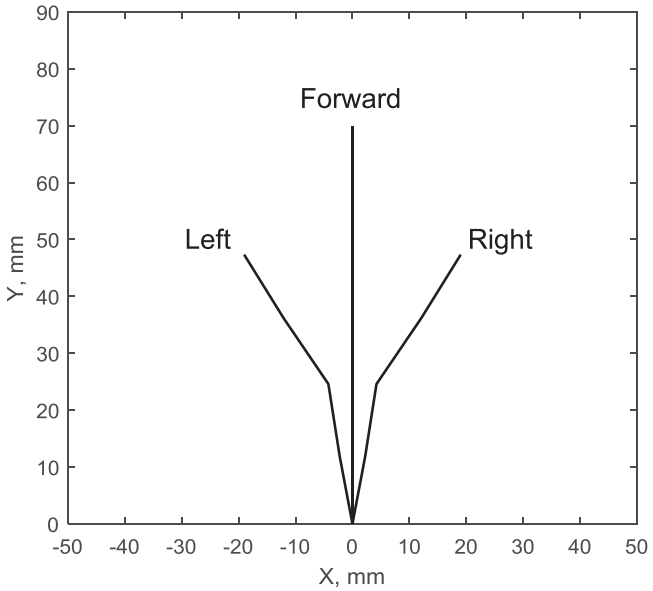

Figure 9. Directional (2D) full robot model results for forward expansion and left ($\phi_R = 2\phi_L$) and right ($\phi_L = 2\phi_R$) turning.

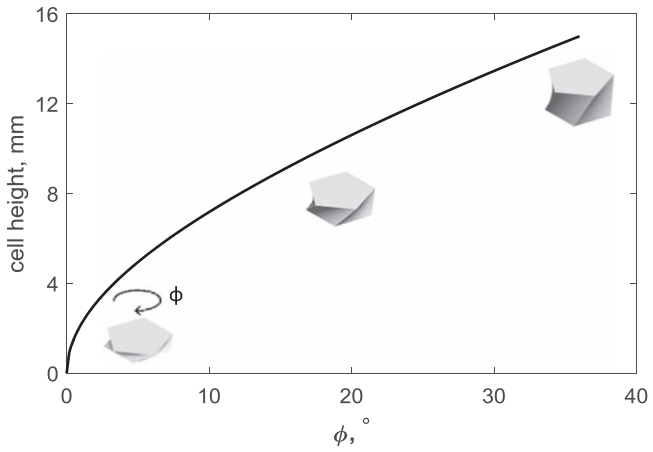

Figure 10. Kinematic model of the Kresling cell height as a function of input rotation, ϕ, applied to the cell, considering only geometry.

4.1. Kinematic model

Figure 10 presents the kinematic model results for a single Kresling cell. The kinematic model is produced from a geometric analysis of the Kresling cell adapted from Pagano et al [3, 18]. The kinematic model outputs the height of the Kresling cell for a given input rotation applied to the cell, ϕ, considering only the geometry of the origami.

The single cell kinematic results presented in figure 10 are extended to the 1D and 2D expansion of the robot front plate using the procedure detailed in section 3.2.1 in the same manner as the dynamic single cell results.

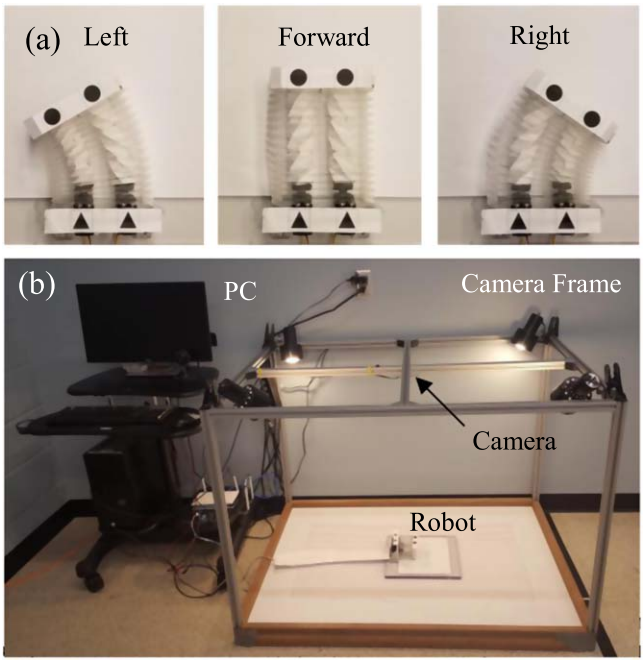

Figure 11. (a) View of robot expansion from the perspective of the camera. (b) System level experimental setup, where the robot back plate was fixed for all tests, and data was collected in a stop-and-stare manner using the markers on the end plates of the robot.

4.2. Experimental setup

Experimental data was collected from the robotic platform Peri using the setup shown in figure 11 and the servo motor inputs given in table 1, where ϕ_L and ϕ_R are the angular rotations applied by the servo motors to the left and right origami towers, respectively, at an angular velocity of 120 rpm. This same angular velocity was used for all model simulations.

With the back plate of the robot fixed, the 2D expansion of the front plate (mass 66.2 g) was recorded by capturing the position of markers on the end plates of the robot using a top view camera, as shown in figure 11(a). The camera recorded the front plate position in a stop-and-stare manner, with the robot pausing after each servo input pair for data collection. The servo input pairs are shown in table 1 (supplementary videos M3, M4, M5).

4.3. Model and experimental results comparison

The 1D expansion results for the full robot dynamic model, kinematic model, and experiment are presented in figure 12. For small motor input rotations, the kinematic model demonstrates greater accuracy tracking the robot locomotion. However, as the robot expands further, the system losses become significant, and the dynamic model agrees with experimental values more closely than the kinematic model. Figure 13(a) shows the 2D dynamic model results compared to the kinematic model and experimental data.

Figure 13(b) shows the error of the dynamic and kinematic models at each expansion step compared to experimental results. The error is defined as the distance between

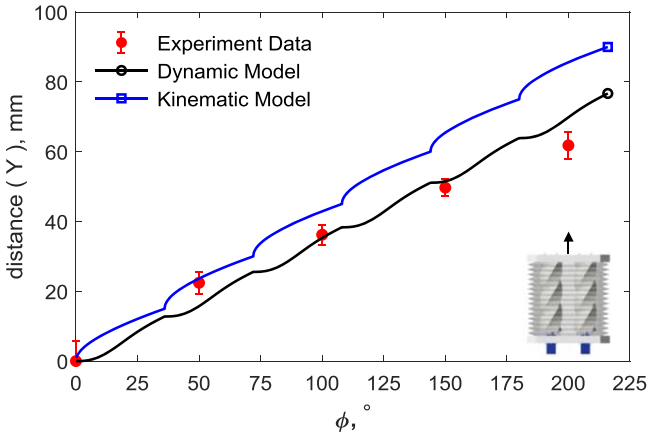

Figure 12. 1D expansion results for the full robot dynamic model compared to experimental data and the kinematic model, where $\phi_L = \phi_R = \phi$.

Table 1. Servo motor rotations for forward, left, and right locomotion of the crawling robot, Peri. Each row corresponds to one step of the robot between pauses for data collection, and ϕ_L and ϕ_R are the servo motor inputs to the left and right origami towers, respectively.

Step #	Forward		Left		Right	
	ϕ_L	ϕ_R	ϕ_L	ϕ_R	ϕ_L	ϕ_R
0	0°	0°	0°	0°	0°	0°
1	50°	50°	25°	50°	50°	25°
2	100°	100°	50°	100°	100°	50°
3	150°	150°	75°	150°	150°	75°
4	200°	200°	100°	200°	200°	100°

the modeled and experimental front plate positions for a given expansion step, expressed as a percentage of the maximum robot expansion. For both forward expansion and turning, the kinematic model demonstrates a greater tracking accuracy than the dynamic model for low motor input rotations. However, as the robot expands further and the system losses increase, the kinematic model becomes increasingly inaccurate, while the dynamic model error remains consistent.

5. Model-based design of robot parameters

The purpose of the dynamic model is to be used for model-based design of origami-enabled robots. This section details how the dynamic model developed for Peri can be used to tune the robot design parameters to achieve desired performance requirements.

Consider the stiffness of the bellows structure. As the bellows stiffness is increased, the robot can achieve further forward locomotion, as shown by the simulations run using the dynamic model and presented in figure 14. However, the increased forward locomotion is accompanied by a decrease in the turning curvature of the robot.

This trade-off between forward locomotion and turning curvature creates a Pareto front for the performance of the

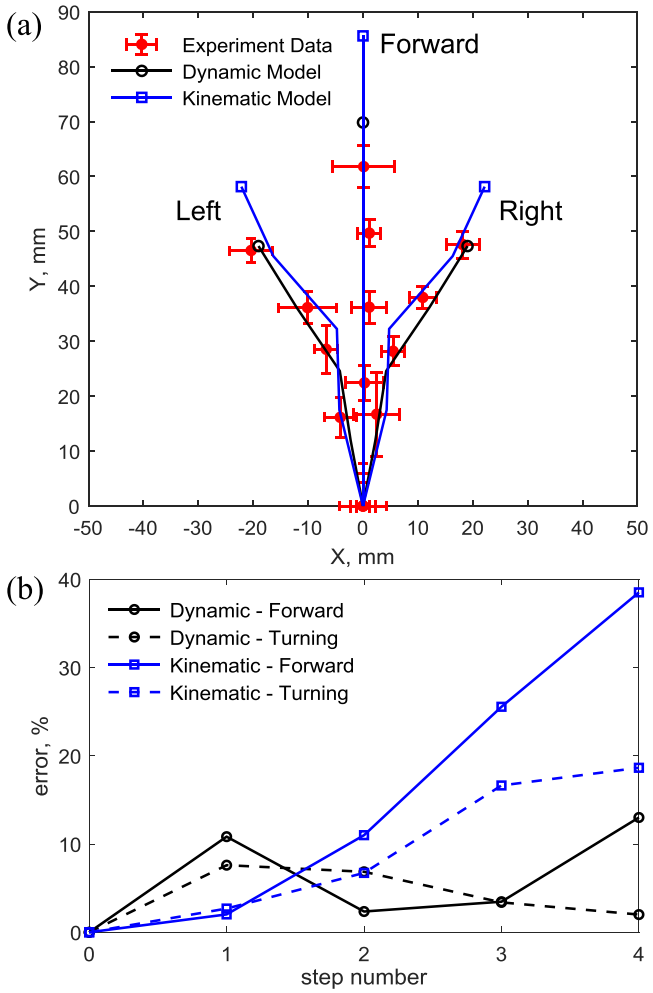

Figure 13. (a) 2D expansion results for the dynamic model, kinematic model, and experiment. (b) Error of the dynamic and kinematic models at each expansion step of the robot expressed as a percentage of the maximum robot expansion, showing the superior locomotion tracking of the dynamic model as the system losses increase.

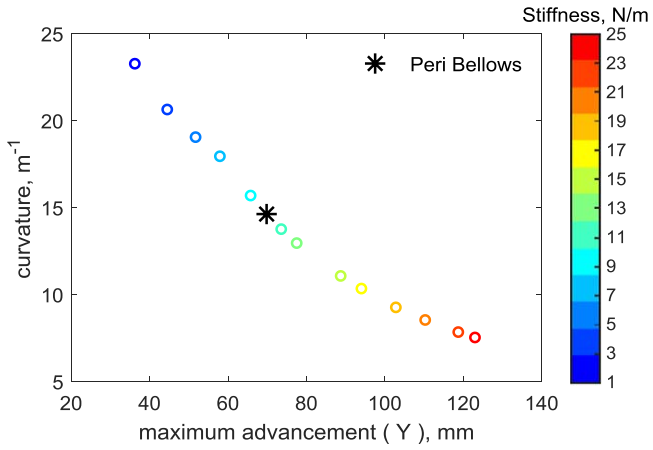

Figure 14. Dynamic model Pareto front of the bellows stiffness trade-off between forward locomotion of the robot and the robot turning curvature, where a higher bellows stiffness increases forward locomotion but limits the robot turning curvature.

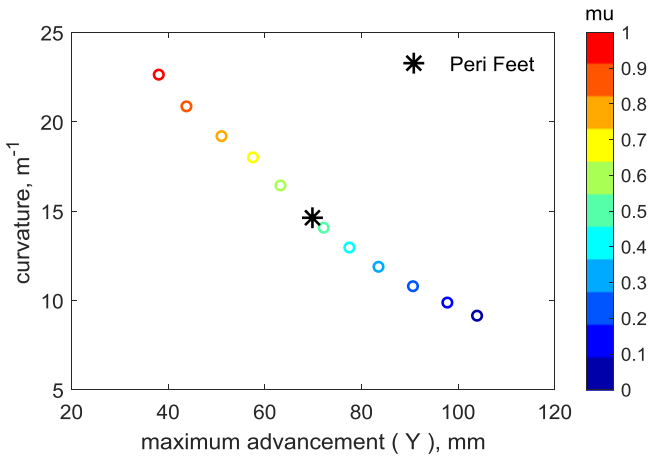

Figure 15. Dynamic model Pareto front of the friction trade-off between forward locomotion of the robot and the robot turning curvature, where a higher coefficient of friction allows for improved robot turning radius but impedes forward locomotion.

robot, for which the bellows stiffness can be tuned. For a certain desired performance, the dynamic model Pareto front presented in figure 14 can be used to select the ideal bellows stiffness.

The same analysis is performed for the coefficient of friction for the feet of Peri. Figure 15 is the Pareto front for the anisotropic feet design, demonstrating that higher friction impedes the forward locomotion of the robot, but allows for a tighter turning radius. Once again, from the Pareto front, the ideal coefficient of friction can be selected depending on whether a tight turning radius or maximum forward expansion is more desirable.

6. Discussion and conclusions

The dynamic model developed in this paper is formulated from an energy analysis of the origami-enabled crawling robot Peri. While a kinematic model of the robot more accurately tracks the robot locomotion for small forward expansions, the dynamic model demonstrates superior locomotion tracking capabilities over the kinematic model as the system losses increase.

The dynamic model performs effectively despite some notable simplifications made in its formulation. The model cannot consider the moment of inertia of the robot end plates, because turning is achieved through the assymetric expansion of single degree of freedom origami cells. In addition, the model assumes that the robot contraction matches the robot expansion, which is likely not a perfect assumption due to the different masses of the robot end plates. This dynamic model creates a framework with opportunities to be refined through further theoretical considerations.

The dynamic model is shown to be beneficial in the design of origami-enabled robotic systems and the tuning of system parameters. Employing a dynamic model to select the ideal design parameters for desired performance requirements eliminates the ad hoc methods currently used to design

origami-enabled robotic systems, and can lead to more optimal system designs in a more efficient and timely manner.

While the dynamic model developed in this paper is tailored specifically for the robotic platform Peri, it establishes a much-needed framework that can be extended to other origami-enabled robotic systems. The ability to create a system level model for origami-enabled robots that synergistically integrates the origami structure into the system performance can lead to advances in the design and control of pseudo-compliant origami-enabled robots.

Acknowledgments

The authors are grateful to Dr Andrew Alleyne for his contributions to the technical discussions that guided the direction of this research. The authors also appreciate support from the Mechanical Science and Engineering department and the Materials Testing Laboratory at the University of Illinois at Urbana-Champaign.

ORCID iDs

Aimy Wissa https://orcid.org/0000-0002-8468-511X

References

[1] Rus D and Tolley M T 2018 Design, fabrication and control of origami robots *Nat. Rev. Mater.* **3** 101–12
[2] Zhakypov Z and Paik J 2018 Design methodology for constructing multimaterial origami robots and machines *IEEE* **34** 151–65
[3] Pagano A, Yan T, Chien B, Wissa A and Tawfick S 2017 A crawling robot driven by multi-stable origami *Smart Mater. Struct.* **26** 094007
[4] Schenk M and Guest S D 2013 Geometry of Miura-folded metamaterials *Proc. Natl Acad. Sci.* **110** 3276–81
[5] Li S and Wang K W 2015 Fluidic origami with embedded pressure dependent multi-stability: a plant inspired innovation *J. R. Soc. Interface* **12** 20150639
[6] Filipov E T, Paulino G H and Tachi T 2016 Origami tubes with reconfigurable polygonal cross-sections *Proc. R. Soc.* A **472** 20150607
[7] Saito K, Tsukahara A and Okabe Y 2016 Designing of self-deploying origami structures using geometrically misaligned crease patterns *Proc. R. Soc.* A **472** 20150235
[8] Liu K and Paulino G H 2017 Nonlinear mechanics of non-rigid origami: an efficient computational approach *Proc. R. Soc.* A **473** 20170348
[9] Zhai Z, Wang Y and Jiang H 2018 Origami-inspired, on-demand deployable and collapsible mechanical metamaterials with tunable stiffness *Proc. Natl Acad. Sci.* **115** 2032–7
[10] Fang H, Zhang Y and Wang K W 2017 Origami-based earthworm-like locomotion robots *Bioinspir. Biomim.* **12** 065003
[11] Onal C D, Wood R J and Rus D 2012 An Origami-inspired approach to worm robots *IEEE* **18** 430–8
[12] Virgala I, Gmiterko A and Kelemen M 2013 Motion analysis of in-pipe robot based on SMA spring actuator *J. Autom. Control* **1** 21–5
[13] Daynes S, Trask R S and Weaver P M 2014 Bio-inspired structural bistability employing elastomeric origami for morphing applications *Smart Mater. Struct.* **23** 125011
[14] Felton S M, Tolley M T, Shin B, Onal C D, Demaine E D, Rus D and Wood R J 2013 Self-folding with shape memory composites *Soft Matter* **9** 7688–94
[15] Sun X, Felton S M, Niiyama R, Wood R J and Kim S 2015 Self-folding and self-actuating robots: a pneumatic approach *IEEE Int. Conf. on Robotics and Automation, Seattle, WA* (https://doi.org/10.1109/ICRA.2015.7139634)
[16] Tachi T and Hull T C 2017 Self-foldability of rigid origami *J. Mech. Robot.* **9** 021008
[17] Angatkina O, Gustafson K, Wissa A and Alleyne A 2019 Path following for the soft origami crawling robot *Dynamic Systems and Control Conf., Park City, UT*
[18] Angatkina O, Chien B, Pagano A, Yan T, Alleyne A, Tawfick S and Wissa A 2017 A metameric crawling robot enabled by origami and smart materials *Conf. on Smart Materials, Adaptive Structures and Intelligent Systems, Snowbird, UT* (https://doi.org/10.1115/SMASIS2017-3836)